The Journal of Chemical Physics ARTICLE scitation.org/journal/jcp

# Static polarizabilities within the generalized Kohn–Sham semicanonical projected random phase approximation (GKS-spRPA)

Cite as: J. Chem. Phys. 157, 164107 (2022); doi: 10.1063/5.0103664
Submitted: 16 June 2022 • Accepted: 26 September 2022 •
Published Online: 26 October 2022



Sree Ganesh Balasubramani,[1,2] Vamsee K. Voora,[2,a)] and Filipp Furche[2,b)]

## AFFILIATIONS

[1] Department of Chemistry and Biochemistry, University of Arizona, 1306 East University Blvd., Tucson, Arizona 85721, USA
[2] Department of Chemistry, University of California, Irvine, 1102 Natural Sciences II, Irvine, California 92697-2025, USA

[a)] **Present address:** Department of Chemical Sciences, Tata Institute of Fundamental Research, Homi Bhabha Road, Colaba, Mumbai 400005, India.
[b)] **Author to whom correspondence should be addressed:** filipp.furche@uci.edu

## ABSTRACT

An analytical implementation of static dipole polarizabilities within the generalized Kohn–Sham semicanonical projected random phase approximation (GKS-spRPA) method for spin-restricted closed-shell and spin-unrestricted open-shell references is presented. General second-order analytical derivatives of the GKS-spRPA energy functional are derived using a Lagrangian approach. By resolution-of-the-identity and complex frequency integration methods, an asymptotic $\mathcal{O}(N^4 \log(N))$ scaling of operation count and $\mathcal{O}(N^3)$ scaling of storage is realized, i.e., the computational requirements are comparable to those for GKS-spRPA ground state energies. GKS-spRPA polarizabilities are assessed for small molecules, conjugated long-chain hydrocarbons, metallocenes, and metal clusters, by comparison against Hartree–Fock (HF), semilocal density functional approximations (DFAs), second-order Møller–Plesset perturbation theory, range-separated hybrids, and experimental data. For conjugated polydiacetylene and polybutatriene oligomers, GKS-spRPA effectively addresses the "overpolarization" problem of semilocal DFAs and the somewhat erratic behavior of post-PBE RPA polarizabilities without empirical adjustments. The ensemble averaged GKS-spRPA polarizabilities of sodium clusters ($Na_n$ for $n = 2, 3, \ldots, 10$) exhibit a mean absolute deviation comparable to PBE with significantly fewer outliers than HF. In conclusion, analytical second-order derivatives of GKS-spRPA energies provide a computationally viable and consistent approach to molecular polarizabilities, including systems prohibitive for other methods due to their size and/or electronic structure.



## I. INTRODUCTION

The dipole moment and the static polarizability are fundamental molecular properties defined by the linear and quadratic response of the energy $E$ with respect to a uniform electric field $\mathcal{F}$[1,2]

$$E(\mathcal{F}) = E_0 - \boldsymbol{\mu} \cdot \mathcal{F} + \frac{1}{2}\mathcal{F} \cdot \boldsymbol{\alpha} \cdot \mathcal{F} + O(\mathcal{F}^3), \quad (1)$$

where $E_0$ is the unperturbed ground state energy, $\boldsymbol{\mu}$ is the dipole moment, and $\boldsymbol{\alpha}$ is the static polarizability tensor. Accurate *ab initio* calculation of electronic polarizabilities requires a balanced description of electron correlation[3] and suitable basis sets;[4–7] moreover, vibrational, rotational, and thermal contributions to total molecular polarizabilities can be significant.[8] Wavefunction-based response methods within the Hartree–Fock (HF) framework,[9–11] second-order Møller–Plesset (MP2) perturbation theory,[12,13] and approximate coupled cluster theory (CC) methods, such as CC singles and doubles (CCSD), CCSD with perturbative triples [CCSD(T)],[14,15] CC2[16] and CC3[17] methods, have been demonstrated to yield highly accurate static polarizabilities for systems whose ground state is dominated by the HF reference. With the exception of HF, these approaches include electron correlations at various levels of approximations, but can be computationally expensive for large molecular systems, particularly in conjunction with diffuse-augmented basis sets.[18]

Density functional approximations (DFAs)[19,20] within the Kohn–Sham (KS)[21] or the generalized KS (GKS)[22] framework are widely used to compute molecular polarizabilities[23–25] due to

their computational efficiency. Nevertheless, one of the widely known shortcomings of semilocal (SL) DFAs is their tendency to massively overestimate polarizabilities of conjugated systems.[26–29] This somewhat unexpected failure of semilocal DFAs has been rationalized by an ultranonlocal "field counteracting" term in the exact exchange–correlation (XC) potential not captured by semilocal DFAs.[27,30] This deficiency may be viewed as a form of self-interaction error[31,32] or violation of the fractional charge condition.[33]

Over the past decades, significant effort has been devoted toward rectifying the DFA errors in static polarizabilities, although with varying levels of success.[29,34–37] A popular workaround is the use of hybrid functionals, which include a fraction of HF exchange.[24,38] Garza *et al.*,[39] found static polarizabilities obtained from range-separated hybrid (RSH) functionals to be more accurate than SL DFA ones for long-range charge transfer systems. However, Nénon *et al.* concluded[37] that not only long-range exchange but also long-range correlations are vital for obtaining accurate polarizabilities of large conjugated molecular systems. "Tuning" of RSH functionals[40] improves the nonlinear polarizabilities of certain push–pull systems but is not universally reliable.[41] In practice, one often finds that the polarizabilities of conjugated systems are so sensitive to the amount of HF exchange that one needs to proceed with caution while using these DFAs for polarizability calculations.

Here, we investigate whether the random phase approximation (RPA) for the ground-state correlation energy[42–44] can overcome the overpolarization problem of SL and hybrid DFAs. RPA includes the full HF exchange plus nonlocal long-range correlation and hence does not rely on error cancellation between exchange and correlation as do hybrid and SL DFAs. So far, RPA has mainly been applied to energies and first-order properties in a post-KS fashion[45–48] starting, e.g., from a PBE calculation, but the recent development of self-consistent RPA methods[49] with much diminished dependence on the KS reference motivates this exploration of second-order RPA properties. The computational cost of RPA is higher than that of hybrid DFAs, but comparable to that of a fast MP2 calculation.[44,50] We focus on the GKS semicanonical projected RPA (GKS-spRPA) method, which achieves full orbital stationarity while systematically improving properties such as KS orbital energies, densities, interaction energies, and stability of the GKS reference compared to post-KS RPA.[51] The latter is paramount for second- and higher-order static response properties, which are closely related to the second variation of the ground-state energy functional. Apart from conjugated systems, the performance of RPA response properties for open-shell transition metal compounds and metallic systems is of particular interest for applications to linear and nonlinear optical properties, where HF and MP2 polarizabilities are unreliable.[52,53]

Here, we present the first derivation and implementation of analytical second-order properties, specifically static polarizabilities, within the GKS-spRPA framework. We aim to understand if GKS-spRPA, which includes HF exchange as well as long-range nonlocal correlations, can address the problem of overpolarization affecting SL/hybrid DFAs when calculating static polarizabilities of $\pi$ - conjugated polymers. Furthermore, we test the accuracy of GKS-spRPA static polarizabilities for metallocenes and small metal clusters where the HF reference is qualitatively incorrect and HF-based single-reference approaches such as MP2 are suspect.[52,53] In Sec. II, we briefly review the GKS-spRPA working equations. Next, analytical expressions for second-order properties are developed using a Lagrangian approach, which uses resolution-of-the-identity (RI) factorization of the Coulomb interaction[54] and imaginary frequency integration.[50] The latter bypass explicit calculation of any four-index arrays such as (perturbed) doubles amplitudes or four-center integral derivatives encountered, e.g., in conventional analytical second-order MP2 derivative theory,[55–57] somewhat reminiscent of Laplace-transform RI-MP2 approaches.[16] The main result is an iterative implementation of GKS-spRPA polarizabilities exhibiting the same $O(N^4 \log N)$ scaling as RPA single-point energies. Section IV presents GKS-spRPA static polarizabilities of small molecules, conjugated systems, metallocenes, and metal clusters and compares them to other theoretical and/or experimental results. Furthermore, the basis set and numerical frequency grid convergence behavior of the method are assessed. Conclusions from a theoretical and computational viewpoint are presented in Sec. V.

## II. THEORY

### A. Overview of the GKS-spRPA method

In finite basis set calculations, the spin-unrestricted KS or GKS molecular orbitals (MOs) $\{\phi_{p\sigma}\}$ are linear combinations of basis functions $\{\chi_\mu\}$,

$$\phi_{p\sigma}(\mathbf{r}) = \sum_\mu C_{\mu p\sigma}\chi_\mu(\mathbf{r}). \tag{2}$$

In molecular applications, the basis functions $\{\chi_\mu\}$ are typically atom-centered "atomic orbitals" (AOs), giving rise to a nondiagonal overlap matrix

$$S_{\mu\nu} = \int d^3r\, \chi_\mu(\mathbf{r})\chi_\nu(\mathbf{r}). \tag{3}$$

Throughout this paper, indices $i, j, \ldots$ denote occupied $a, b, \ldots$ virtual (unoccupied), and $p, q, \ldots$ general MOs, whereas atomic orbital basis functions are denoted by Greek indices $\mu, \nu, \ldots$, localized auxiliary basis functions are denoted by capital Roman indices $P, Q, \ldots$, and $\sigma = \alpha, \beta$ is a spin index. We consider real MOs and spin-unrestricted references in this paper. The MO coefficients $\mathbf{C}_\sigma$ are solutions of the canonical (G)KS equation[51]

$$\mathbf{H}_\sigma^{\mathrm{KS}}[\mathbf{D}_\alpha, \mathbf{D}_\beta]\mathbf{C}_\sigma = \mathbf{S}\mathbf{C}_\sigma\boldsymbol{\varepsilon}_\sigma, \tag{4}$$

under the orthonormality constraint

$$\mathbf{C}^\dagger\mathbf{S}\mathbf{C} = \mathbf{1}, \tag{5}$$

and $\boldsymbol{\varepsilon}_\sigma$ is the diagonal matrix of the orbital energies. The KS or GKS Hamiltonian $\mathbf{H}_\sigma^{\mathrm{KS}}[\mathbf{D}_\alpha, \mathbf{D}_\beta] = \mathbf{h}_\sigma + \mathbf{V}_\sigma^{\mathrm{HXC}}[\mathbf{D}_\alpha, \mathbf{D}_\beta]$ may be separated into a "core" Hamiltonian $\mathbf{h}_\sigma$ containing the one-electron operators of the kinetic energy, the electron-nucleus attraction, as well as additional terms arising from static external electric or magnetic fields. The Hartree, exchange, and correlation (HXC) potential $\mathbf{V}_\sigma^{\mathrm{HXC}} = \mathbf{V}^{\mathrm{H}} + \mathbf{V}_\sigma^{\mathrm{XC}}$ arises from a local multiplicative HXC potential in the strict KS approach, whereas in GKS theory, the

exchange–correlation potential is generally nonlocal.[22,58] The $\sigma$-spin (G)KS one-particle density matrix

$$\mathbf{D}_\sigma = \mathbf{C}_\sigma \mathbf{n}_\sigma \mathbf{C}_\sigma^\dagger \tag{6}$$

contains the occupation number matrix $\mathbf{n}_\sigma$ which, for pure states, is diagonal with eigenvalues 1 for occupied and 0 for virtual MOs. The occupation numbers are usually chosen such that the canonical KS orbitals and their energy eigenvalues satisfy the Aufbau principle. In the following we use the short-hand notation $\mathbf{D} = \{\mathbf{D}_\alpha, \mathbf{D}_\beta\}$, $\mathbf{C} = \{\mathbf{C}_\alpha, \mathbf{C}_\beta\}$ and $\boldsymbol{\varepsilon} = \{\boldsymbol{\varepsilon}_\alpha, \boldsymbol{\varepsilon}_\beta\}$ for convenience.

Once the KS MOs and orbital energies are determined, the RPA energy is obtained as the sum of the HF or HX energy $E^{\mathrm{HF}}[\mathbf{D}]$ and the RPA correlation energy $E^{\mathrm{C\,RPA}}$,[59]

$$E^{\mathrm{RPA}}[\mathbf{D}] = E^{\mathrm{HF}}[\mathbf{D}] + E^{\mathrm{C\,RPA}}[\mathbf{D}]. \tag{7}$$

Within the RI approximation and using imaginary-axis frequency integration,[50] the RIRPA correlation energy is given by

$$E^{\mathrm{C\,RIRPA}}[\mathbf{D}] = \frac{1}{2}\int_\infty^\infty \frac{d\omega}{2\pi} \langle \ln(\mathbf{1} + \mathbf{Q}(\omega)) - \mathbf{Q}(\omega) \rangle, \tag{8}$$

where $\langle\cdot\rangle$ denotes the trace operation. The RI approximation[50,54] for direct or Coulomb ($J$) contractions is an approximate factorization of the four-center electron repulsion integrals (ERIs) $\Pi^{(4)}_{\mu\nu\kappa\lambda} = (\mu\nu|\kappa\lambda)$ into lower-rank three- and two-center integrals,

$$\boldsymbol{\Pi}^{(4)}_{\mathrm{RI}} = \boldsymbol{\Pi}^{(3)} \left(\boldsymbol{\Pi}^{(2)}\right)^{-1} \boldsymbol{\Pi}^{(3)T}, \tag{9}$$

where $\Pi^{(3)}_{\mu\nu P} = (\mu\nu|P)$ and $\Pi^{(2)}_{PQ} = (P|Q)$. Here, we use the Mulliken notation for ERIs,

$$(\mu\nu|\kappa\lambda) = \int d^3r_1 d^3r_2 \frac{\chi_\mu(\mathbf{r}_1)\chi_\nu(\mathbf{r}_1)\chi_\kappa(\mathbf{r}_2)\chi_\lambda(\mathbf{r}_2)}{|\mathbf{r}1 - \mathbf{r}2|}. \tag{10}$$

$(\boldsymbol{\Pi}^{(2)})^{-1}$ is calculated via Cholesky decomposition,

$$\left(\boldsymbol{\Pi}^{(2)}\right)^{-1} = \boldsymbol{\Lambda}^T \boldsymbol{\Lambda}, \tag{11}$$

where $\boldsymbol{\Lambda}$ is upper triangular. $\mathbf{Q}(\omega)$ is expressed as

$$\mathbf{Q}(\omega) = 2\mathbf{B}^T \mathbf{G} \mathbf{B}. \tag{12}$$

$\mathbf{G}$ is a frequency dependent supermatrix,

$$\mathbf{G}(\omega) = \boldsymbol{\Delta}(\boldsymbol{\Delta}^2 + \omega^2 \mathbf{1})^{-1}, \tag{13}$$

where $\boldsymbol{\Delta}$ in a general non-canonical basis is expressed as

$$\Delta_{ia\sigma\, jb\sigma'} = \delta_{\sigma\sigma'}(\varepsilon_{ab\sigma}\delta_{ij} - \varepsilon_{ij\sigma'}\delta_{ab}), \tag{14}$$

and $\mathrm{B}_{ia\sigma P}$ is defined as

$$\mathrm{B}_{ia\sigma P} = \sum_{\mu\nu Q} C_{\mu i\sigma} C_{\nu a\sigma} (\mu\nu|P) (\boldsymbol{\Lambda})^{-1}_{QP}. \tag{15}$$

The Post-KS RPA method depends explicitly on the reference semilocal (SL) KS potential and orbitals. SL KS potentials are known to be inaccurate for describing the electronic structure of open-shell molecules, anions, and small-gap compounds.[60,61] Furthermore, the post-KS RPA energy functional is not variationally stable because of this dependence. To address such issues, Voora *et al.*[51] devised an orbital self-consistent method called the GKS-spRPA, which variationally extremizes the spRPA energy $E^{\mathrm{spRPA}}[\mathbf{D}, \tilde{\mathbf{H}}^{\mathrm{KS}}]$ with respect to the GKS density matrix. The spRPA energy functional $E^{\mathrm{spRPA}}[\mathbf{D}, \tilde{\mathbf{H}}^{\mathrm{KS}}]$ implicitly depends on $\mathbf{h}, \boldsymbol{\Pi}^{(2)}, \boldsymbol{\Pi}^{(3)}$ and $\boldsymbol{\Pi}^{(4)}$. In general, the GKS density matrix can be defined as

$$\mathbf{D} = \sum_{\lambda,\lambda'} P_\lambda \mathbf{n}_{\lambda\lambda'} P_{\lambda'}, \tag{16}$$

where $P_\lambda$ are orthogonal projectors, which project onto the space of KS orbitals with degenerate occupation numbers, and $\mathbf{n}_{\lambda\lambda'} = \mathbf{n}_\lambda \delta_{\lambda\lambda'}$ is diagonal with $\mathbf{n}_\lambda$ denoting the occupation number matrix of the $\lambda$ block. For the case of integer orbital occupation numbers, the $\mathbf{n}_\lambda$ matrices have two distinct eigenvalues, 0 and 1. The sp KS Hamiltonian is defined in terms of the semilocal KS Hamiltonian as

$$\tilde{\mathbf{H}}^{\mathrm{KS}} = \sum_\lambda P_\lambda \mathbf{H}^{\mathrm{KS\,SL}} P_\lambda. \tag{17}$$

$\mathbf{D}$ and $\tilde{\mathbf{H}}^{\mathrm{KS}}$ commute by construction and a common set of "semicanonical" basis can be determined. The GKS-spRPA effective one particle Hamiltonian is given by

$$\begin{aligned}\mathbf{H}^{\mathrm{spRPA}}_\sigma[\mathbf{D}, \tilde{\mathbf{H}}^{\mathrm{KS}}] &= \frac{\partial E^{\mathrm{spRPA}}[\mathbf{D}, \tilde{\mathbf{H}}^{\mathrm{KS}}]}{\partial \mathbf{D}_\sigma} \\ &= \mathbf{H}^{\mathrm{HF}}_\sigma[\mathbf{D}] + \mathbf{V}^{\mathrm{c\,spRPA}}_\sigma[\mathbf{D}, \tilde{\mathbf{H}}^{\mathrm{KS}}],\end{aligned} \tag{18}$$

where $\mathbf{H}^{\mathrm{HF}}_\sigma[\mathbf{D}]$ is the Hartree–Fock Hamiltonian and $\mathbf{V}^{\mathrm{c\,spRPA}}_\sigma[\mathbf{D}, \tilde{\mathbf{H}}^{\mathrm{KS}}]$ corresponds to the nonlocal GKS-spRPA correlation potential. To determine the optimized orbitals, it is sufficient to make the occupied-virtual block of $\mathbf{H}^{\mathrm{spRPA}}_\sigma$ vanish according to Brillouin's theorem.[62] The occupied-virtual block of $\mathbf{H}^{\mathrm{spRPA}}_\sigma$ is given by[51]

$$\mathrm{H}^{\mathrm{spRPA}}_{ia\sigma} = \mathrm{H}^{\mathrm{HF}}_{ia\sigma} + \gamma_{ia\sigma} - \gamma_{ai\sigma} + H^+_{ia\sigma}[\mathbf{T}_\sigma] + [\mathbf{T}_\sigma, \boldsymbol{\varepsilon}_\sigma]_{ia}, \tag{19}$$

where $H^+$ denotes the first-order HXC potential,[63] $\mathbf{T}_\sigma$ is the GKS-spRPA unrelaxed difference density matrix[45]

$$\mathbf{T}_\sigma = \frac{\partial E^{\mathrm{spRPA}}}{\partial \boldsymbol{\varepsilon}_\sigma}, \tag{20}$$

whose occupied-virtual and virtual-occupied blocks are zero. The occupied–occupied and virtual–virtual blocks of $\mathbf{T}_\sigma$ can be expressed as

$$\mathrm{T}_{ij\sigma} = \int_{-\infty}^\infty \frac{d\omega}{2\pi} \sum_a (\mathbf{M}(\omega) - \omega^2 \boldsymbol{\Delta}^{-1}\mathbf{M}(\omega)\boldsymbol{\Delta}^{-1})_{ia\sigma\, ja\sigma}, \tag{21}$$

$$T_{ab\sigma} = \int_{-\infty}^{\infty} \frac{d\omega}{2\pi} \sum_i (\mathbf{M}(\omega) - \omega^2 \boldsymbol{\Delta}^{-1} \mathbf{M}(\omega) \boldsymbol{\Delta}^{-1})_{ia\sigma\, ib\sigma}, \tag{22}$$

where

$$\mathbf{M}(\omega) = \mathbf{G}\mathbf{B}\tilde{\mathbf{Q}}\mathbf{B}^T\mathbf{G}, \tag{23}$$

and $\tilde{\mathbf{Q}}$ is given by

$$\tilde{\mathbf{Q}} = (\mathbf{1} + \mathbf{Q})^{-1} - \mathbf{1}. \tag{24}$$

The matrix elements of $\boldsymbol{\gamma}$ are obtained as[45]

$$\begin{aligned} \gamma_{ap\sigma} &= 2 \int_{-\infty}^{\infty} \frac{d\omega}{2\pi} \sum_j (\mathbf{G}\mathbf{B}\tilde{\mathbf{Q}}\mathbf{B}^T)_{ja\sigma\, jp\sigma}, \\ \gamma_{ip\sigma} &= 2 \int_{-\infty}^{\infty} \frac{d\omega}{2\pi} \sum_b (\mathbf{G}\mathbf{B}\tilde{\mathbf{Q}}\mathbf{B}^T)_{ib\sigma\, pb\sigma}. \end{aligned} \tag{25}$$

### B. The GKS-spRPA energy Lagrangian

To determine molecular properties, we consider the first and second-order response of the GKS-spRPA ground-state energy with respect to changes in the defining parameters $\mathbf{S}$, $\mathbf{X} = \{\mathbf{h}, \boldsymbol{\Pi}^{(2)}, \boldsymbol{\Pi}^{(3)}, \boldsymbol{\Pi}^{(4)}\}$, and $\mathbf{V}^{\mathrm{XC,SL}} = \{\mathbf{V}_\alpha^{\mathrm{XC,SL}}, \mathbf{V}_\beta^{\mathrm{XC,SL}}\}$.[50,54] We define the GKS-spRPA energy Lagrangian as

$$\begin{aligned} L[\mathbf{C}, \tilde{\mathbf{H}}^{\mathrm{KS}}, \mathbf{T}, \mathbf{W}] = E^{\mathrm{spRPA}}[\mathbf{D}, \tilde{\mathbf{H}}^{\mathrm{KS}}] + \langle \mathbf{T}(\tilde{\mathbf{H}}^{\mathrm{KS}} - \mathbf{H}^{\mathrm{KS\,SL}}[\mathbf{D}] \rangle \\ - \langle \mathbf{W}\mathbf{n}(\mathbf{C}^\dagger \mathbf{S}\mathbf{C} - \mathbf{1}) \rangle. \end{aligned} \tag{26}$$

The MO coefficients $\mathbf{C}$ are the primary variational parameters, and $\mathbf{T}$ and $\mathbf{W}$ are Lagrange multipliers enforcing Eq. (20) and (occupied) MO orthonormality, respectively. The Lagrange multiplier $\mathbf{T}$ constrains the sp Hamiltonian to be $\mathbf{H}^{\mathrm{KS\,SL}}$. The density matrix $\mathbf{D}$ depends on the MO coefficients and the occupation numbers according to Eq. (6); however, in the present work, we only consider number-conserving variations of $\mathbf{D}$ keeping the occupation numbers $\mathbf{n}$ constant at their ground-state values; for properties related to changes in particle numbers such as ionization potentials or electron affinities, the reader is referred to Refs. 64 and 65. Furthermore, the Lagrangian parametrically depends on $\mathbf{n}$, $\mathbf{S}$, $\mathbf{X}$, and $\mathbf{V}^{\mathrm{XC,SL}}$.

The GKS-spRPA energy Lagrangian is constructed to be stationary at the GKS-spRPA ground-state solution. The stationarity condition with respect to the MO coefficients $\mathbf{C}$,

$$\frac{\partial L[\mathbf{C}, \tilde{\mathbf{H}}^{\mathrm{KS}}, \mathbf{T}, \mathbf{W} | \mathbf{n}, \mathbf{S}, \mathbf{X}, \mathbf{V}^{\mathrm{XC,SL}}]}{\partial \mathbf{C}} = \mathbf{0}, \tag{27}$$

reduces to the GKS-spRPA Eq. (4) for $\mathbf{n}\mathbf{W} = \boldsymbol{\varepsilon}$; the Lagrange multiplier $\mathbf{W}$ is thus the GKS-spRPA "energy weighted density matrix" familiar from analytical gradient theory.[66] By construction, $L$ equals the GKS-spRPA ground-state energy at its stationary point ($E_0$),

$$\begin{aligned} &L[\mathbf{C}, \tilde{\mathbf{H}}^{\mathrm{KS}}, \mathbf{T}, \mathbf{W} | \mathbf{n}, \mathbf{S}, \mathbf{X}, \mathbf{V}^{\mathrm{XC,SL}}]\big|_{\mathrm{stat}} \\ &\quad = E^{\mathrm{spRPA}}[\mathbf{D}_{\mathrm{stat}}, \tilde{\mathbf{H}}^{\mathrm{KS}}[\mathbf{D}_{\mathrm{stat}}] | \mathbf{S}, \mathbf{X}, \mathbf{V}^{\mathrm{XC,SL}}] \\ &\quad = E_0[\mathbf{S}, \mathbf{X}, \mathbf{V}^{\mathrm{XC,SL}}], \end{aligned} \tag{28}$$

where the subscript "stat" means that all variables are at their stationary ground-state values.

Equation (28) greatly simplifies the computation of GKS-spRPA energy derivatives due to the stationarity of $L$. For example, the energy gradient with respect to a perturbation $\xi$ is[45]

$$\begin{aligned} \frac{dE^{\mathrm{spRPA}}[\mathbf{S}, \mathbf{X}, \mathbf{V}^{\mathrm{XC,SL}}]}{d\xi} &= \left\langle \frac{\partial L}{\partial \mathbf{S}}\bigg|_{\mathrm{stat}} \mathbf{S}^\xi \right\rangle + \left\langle \frac{\partial L}{\partial \mathbf{X}}\bigg|_{\mathrm{stat}} \mathbf{X}^\xi \right\rangle \\ &\quad + \left\langle \frac{\partial L}{\partial \mathbf{V}^{\mathrm{XC,SL}}}\bigg|_{\mathrm{stat}} \mathbf{V}^{\mathrm{XC,SL}\xi} \right\rangle. \end{aligned} \tag{29}$$

(We neglect derivatives of frequency quadrature nodes and weights; see Appendix B of Ref. 45 for further details.) Derivatives of matrices with respect to perturbations $\{\xi\}$ are represented using superscript $\{\xi\}$ for convenience. All derivatives with respect to variational parameters vanish in accordance with Wigner's $2n+1$ and $2n+2$ rules[67,68] The derivative with respect to $\mathbf{X}$ in Eq. (29) may be expressed as

$$\frac{\partial L}{\partial \mathbf{X}}\bigg|_{\mathrm{stat}} = \mathbf{P}^{\mathrm{spRPA}}, \tag{30}$$

where $\mathbf{P}^{\mathrm{spRPA}}$ represents the GKS-spRPA generalized n-particle density matrix, and detailed expressions of this matrix are provided in the supplementary material. The derivatives with respect to $\mathbf{S}$ and $\mathbf{V}^{\mathrm{XC,SL}}$ are identified as the energy-weighted density matrix $\mathbf{W}$ and the unrelaxed difference density matrix of the unperturbed system,

$$\frac{\partial L}{\partial \mathbf{S}}\bigg|_{\mathrm{stat}} = \mathbf{W}, \quad \frac{\partial L}{\partial \mathbf{V}^{\mathrm{XC,SL}}}\bigg|_{\mathrm{stat}} = \mathbf{T}. \tag{31}$$

Due to the orbital stationarity of the Lagrangian, no orbital relaxation contribution to $\mathbf{T}$ is needed to evaluate the gradient.

### C. Analytical second-order derivatives

Straightforward differentiation of Eq. (28) yields the second analytical derivative of the GKS-spRPA energy with respect to perturbations $\xi$ and $\eta$,

$$\begin{aligned} \frac{\partial^2 E^{\mathrm{spRPA}}}{\partial\eta\partial\xi} &= \left\langle \left( \left( \frac{\partial^2 L}{\partial\eta\partial\mathbf{C}^\dagger} \right) \mathbf{C}^\xi \right\rangle + \left\langle \left( \frac{\partial^2 L}{\partial\eta\partial\mathbf{X}} \right) \mathbf{X}^\xi \right\rangle \right. \\ &\quad + \left\langle \left( \frac{\partial L}{\partial \mathbf{X}} \right) \mathbf{X}^{\eta\xi} \right\rangle + \left\langle \left( \frac{\partial^2 L}{\partial\eta\partial\mathbf{S}} \right) \mathbf{S}^\xi \right\rangle + \left\langle \left( \frac{\partial L}{\partial \mathbf{S}} \right) \mathbf{S}^{\eta\xi} \right\rangle \\ &\quad \left. + \left\langle \left( \frac{\partial^2 L}{\partial\eta\partial\mathbf{V}^{\mathrm{XC,SL}}} \right) \mathbf{V}^{\mathrm{XC,SL}\xi} \right\rangle + \left\langle \left( \frac{\partial L}{\partial \mathbf{V}^{\mathrm{XC,SL}}} \right) \mathbf{V}^{\mathrm{XC,SL}\eta\xi} \right\rangle \right)\Big|_{\mathrm{stat}}. \end{aligned} \tag{32}$$

The first term in Eq. (32) requires the calculation of perturbed MO coefficients $\mathbf{C}^\xi$, which are typically obtained by introducing the ansatz[69]

$$\mathbf{C}(\xi) = \mathbf{C}^{(0)}\mathbf{U}(\xi), \tag{33}$$

where $\mathbf{U}(\xi) = \mathbf{1} + \mathbf{U}^\xi + \cdots$ and $\mathbf{C}^{(0)}$ is the unperturbed MO coefficients matrix. $\mathbf{U}$ is not necessarily unitary;[70] instead it is constrained by the orthonormality condition of the MO coefficients according

to Eq. (5), which may depend on the perturbation(s). The matrix elements of the various blocks of $\mathbf{U}^{\xi}$ are well known from analytic Hessian theory.[71,72] The occupied–occupied block of $\mathbf{U}^{\xi}$ can be obtained in terms of the perturbed overlap matrix as

$$\mathrm{U}^{\xi}_{ij} = -\frac{1}{2}\mathrm{S}^{\xi}_{ij}. \tag{34}$$

The virtual–virtual block of the matrix $\mathbf{U}^{\xi}$ is zero and the occupied-virtual block is obtained as the solution of

$$\sum_{\mu\nu jb}\left(\mathbf{C}^{\dagger}\frac{\partial^2 L}{\partial\mathbf{C}\partial\mathbf{C}^{\dagger}}\mathbf{C}\right)_{iajb}\mathrm{U}^{\xi}_{jb} = -\sum_{\mu}\frac{\partial^2 L}{\partial\xi\partial\,\mathrm{C}_{i\mu}}\mathrm{C}_{\mu a}. \tag{35}$$

The term within parentheses is identified as the symmetric part of the GKS-spRPA orbital rotation Hessian, which is often denoted within time dependent response theory as $(\mathbf{A}+\mathbf{B})$,[73] and accordingly Eq. (35) takes the form

$$(\mathbf{A}+\mathbf{B})\mathbf{U}^{\xi} = \mathbf{RHS}^{\xi}. \tag{36}$$

The matrix elements of the occupied-virtual block of the right hand side ($\mathbf{RHS}$) can be expressed as

$$\mathrm{RHS}^{\xi}_{ia} = \mathrm{H}^{\mathrm{spRPA}\xi}_{ia} - \left(\mathbf{WS}^{\xi}\right)_{ia} - G^{+}_{ia}[\mathbf{S}^{\xi}], \tag{37}$$

where $G^{+}_{\mu\nu\kappa\lambda}$ is defined as

$$G^{+}_{\mu\nu\kappa\lambda} = \frac{\partial W_{\mu\nu}}{\partial\,\mathrm{D}_{\kappa\lambda}}. \tag{38}$$

Here, we consider uniform electric field perturbations whose explicit dependence in the Lagrangian arises only through the core Hamiltonian $\mathbf{h}_{\sigma}$ (for field-independent basis functions). Therefore, derivatives of the parameters $\Pi^{(2)}$, $\Pi^{(3)}$ and $\Pi^{(4)}$, $\mathbf{S}$, $\mathbf{V}^{\mathrm{XC}}$ and $\tilde{\mathbf{H}}$ with respect to the perturbations vanish. Nuclear displacements in an atom-centered basis[71] or field-dependent basis functions, such as gauge-including atomic orbitals,[74,75] which are necessary when magnetic field perturbations are involved, may perturb some or all of the parameters and will be studied elsewhere. The $\eta\xi$ element of GKS-spRPA's static polarizability tensor can be expressed as

$$\frac{\partial^2 E^{\mathrm{spRPA}}}{\partial\eta\partial\xi} = \left\langle\left(\frac{\partial^2 L}{\partial\eta\partial\mathbf{C}^{\dagger}_{\sigma}}\right)_{\mathrm{stat}}\mathbf{C}^{\xi}_{\sigma}\right\rangle + \left\langle\left(\frac{\partial^2 L}{\partial\eta\partial\mathbf{h}_{\sigma}}\right)_{\mathrm{stat}}\mathbf{h}^{\xi}_{\sigma}\right\rangle \tag{39}$$

$$= \left\langle\mathbf{RHS}^{\eta}_{\sigma}\mathbf{U}^{\xi}_{\sigma}\right\rangle + \left\langle\mathbf{D}^{\mathrm{spRPA}\eta}_{\sigma}\boldsymbol{\mu}_{\xi\sigma}\right\rangle, \tag{40}$$

where $\boldsymbol{\mu}_{\xi\sigma}$ is the $\xi$ component of the $\sigma$ - spin dipole moment matrix and the GKS-spRPA one particle density matrix $\mathbf{D}^{\mathrm{spRPA}}_{\sigma}$ is defined as

$$\left.\frac{\partial L}{d\mathbf{h}_{\sigma}}\right|_{\mathrm{stat}} = \mathbf{D}^{\mathrm{spRPA}}_{\sigma}. \tag{41}$$

For uniform electric field perturbations the overlap matrix $\mathbf{S}$ is independent of the field and therefore using Eq. (37), $\mathbf{RHS}^{\eta}_{\sigma} = \mathbf{H}^{\mathrm{spRPA}\eta}_{\sigma}$.

Detailed expressions for the RHS and the GKS-spRPA orbital rotation Hessian are provided in the supplementary material.

## III. IMPLEMENTATION

1. Two index zeroth-order intermediates (independent of the perturbation) such as $\mathrm{T}_{ij\sigma}, \mathrm{T}_{ab\sigma}, \gamma_{ia\sigma}, \gamma_{ai\sigma}, \gamma_{ij\sigma}$, and $\gamma_{ab\sigma}$ are built and stored in memory. The $\mathbf{Q}(\omega)$ matrix is frequency-dependent and is written to file for each frequency grid point $\omega_g$ as $\mathbf{Q}(\omega_g)$.
2. The RHS is built with the zeroth-order intermediates from memory as well as the perturbed first-order intermediates (see the supplementary material for detailed equations). $\mathbf{T}^{\xi}_{\sigma}$ and $\boldsymbol{\mu}_{\eta\sigma}$ are used to get the first contribution to the polarizability as $\alpha_{\xi\eta} = \sum_{ij\sigma}\mathrm{T}^{\xi}_{ij\sigma}\mu_{\eta,ji\sigma} + \sum_{ab}\mathrm{T}^{\xi}_{ab\sigma}\mu_{\eta,ba\sigma}$.
3. Solving Eq. (35) is the most time-consuming part of an analytical static polarizability calculation within the GKS-spRPA. Iterative techniques that avoid storage of the entire orbital rotation Hessian matrix but rather deal with only the product of this matrix with $\mathbf{U}^{\xi}$ are preferred since these matrices can be extremely large and dense.[11,18] Krylov space methods have been successfully applied in this regard,[76–78] and we use a recently developed nonorthonormal extension of it, which exploits the decreasing norm of the residual vectors to boost screening in integral-direct response calculations.[79]
4. The product of the orbital rotation Hessian matrix with $\mathbf{U}^{\xi}$ is constructed on the fly, and the resulting matrix $\mathbf{M}^{\xi}$ is stored in file during each iteration. The $\mathbf{M}^{\xi}$ build consists of several intermediate steps that have a scaling of $\mathcal{O}(N^4 log(N))$ with system size $N$ (see the supplementary material for more details).
5. Once the converged $\mathbf{U}^{\xi}$ and $\mathbf{M}^{\eta}$ matrices are obtained, their contribution to the polarizability is calculated as $\alpha_{\xi\eta} = \sum_{ia\sigma}\mathrm{M}^{\xi}_{ia\sigma}\mathrm{U}^{\eta}_{ai\sigma}$.

This method was implemented in a branch of the TURBOMOLE quantum chemistry program package[80] and is scheduled for future release.

## IV. RESULTS

### A. Basis set convergence

The convergence of GKS-spRPA polarizabilities ($\alpha$ is used to denote the static polarizability tensor in the following sections) with respect to the basis set size was studied for LiF and HCN. The geometries were obtained from experimental results.[81] The basis sets used in this study include def2-SVP, TZVPP, QZVPP, SVPD, TZVPPD, and QZVPPD. The extended def2-QZVPP basis sets, which are constructed by downward extrapolation from the def2-QZVPP basis sets ($1s1p1d1f$ for the elements H–Be and $1s1p1d1f1g$ for all others) as suggested by Rappoport and Furche,[7] were used to approximate the basis set limit. The basis set convergence of GKS-spRPA is compared to that of the HF, PBE, PBE0, MP2, and CC2 methods in Fig. 1. All calculations reported here were performed using the TURBOMOLE program package.[80] The % relative deviation from the basis set limit ($\%\mathrm{RD} = \frac{(\alpha^{method}-\alpha^{reference})}{\alpha^{reference}} \times 100$) in the isotropic static polarizability of LiF using the basis sets def2-SVP, TZVPP,

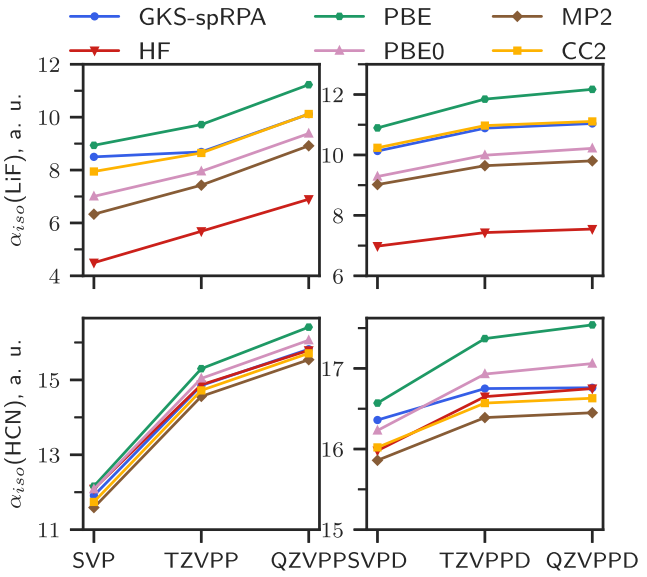


**FIG. 1.** Basis set convergence of the isotropic static polarizability within the GKS-spRPA method for the LiF and HCN molecules, compared to the HF, PBE, PBE0, MP2, and CC2 methods.

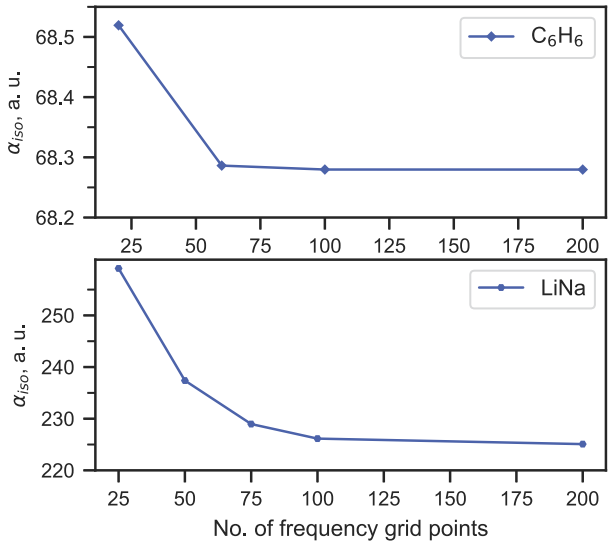


**FIG. 2.** The convergence of the isotropic polarizability within the GKS-spRPA method as a function of the number of frequency grid points for benzene (top) and LiNa (bottom) molecules using the def2-QZVPPD basis and the PBE input orbitals and orbital energies.

QZVPP, SVPD, TZVPPD, and QZVPPD are 23%, 21%, 8%, 8%, 1% and 0.4%, respectively. For the HCN molecule, the %RD for the same order of basis sets are 29%, 12%, 6%, 3%, 0.74%, and 0.71%, respectively. The def2-QZVPPD basis set produces %RD of ≤0.7%, while the def2-TZVPPD basis set results in ≤1% RD compared to the basis set limit in these test calculations. We conclude that the def2-TZVPPD and the def2-QZVPPD basis sets are well suited for calculations of static polarizabilities using the GKS-spRPA method. Moreover, the basis set convergence observed for GKS-spRPA does not differ significantly from that of MP2 or CC2.

## B. Frequency grid convergence

The integration over imaginary frequency in Eq. (8) is done numerically using the Clenshaw-Curtis quadrature with a finite number of grid points as described by Eshuis *et al.*,[50] who used it for computing the RIRPA correlation energy. For polarizability calculations, this is necessary to build several of the zeroth- and first-order intermediates. To test the convergence of the GKS-spRPA static polarizabilities with the number of frequency grid points, we chose to study the $C_6H_6$ and LiNa molecules. The geometries of these molecules were optimized at the level of B3-LYP DFA, the cc-pVTZ basis set, the m4 integration grid, a SCF convergence threshold of $10^{-8}$, and the optimized geometries are provided in the supplementary material. The results of GKS-spRPA static polarizabilities calculated with the def2-QZVPPD basis set and the SL PBE potential as a function of the number of frequency grid points are shown in Fig. 2.

The semicanonical KS HOMO–LUMO gap for the $C_6H_6$ system is 5.13eV, whereas for LiNa, it is 1.31eV. Increasing the number of grid points from 25 to 200 for $C_6H_6$ results in a change in isotropic static polarizability ($\alpha_{iso}$) of 0.24 a.u. (0.4% change), whereas the same increase in the case of LiNa results in a change in $\alpha_{iso}$ of 34.01 a.u. (15% change), as can be seen from Fig. 2. Clearly, systems with a small HOMO–LUMO gap require a large number of frequency grid points to obtain converged static polarizabilities. However, the frequency grids required to reduce the integration error reliably below the inherent method error are comparable to those necessary for first-order analytical derivatives.[45]

## C. Small molecule benchmark

To analyze the accuracy of the GKS-spRPA static polarizabilities and compare them with other quantum chemical methods, we gathered a set of 25 atoms and small molecules. This set consists, among others, of species that are challenging for DFT polarizability predictions as identified by Hait and Head-Gordon.[82] The geometries of these molecules were optimized at the MP2/cc-pVTZ level wherever experimental geometries[81] were not available. A comparison of the GKS-spRPA method with HF, MP2, PBE, and PBE0 is presented in Fig. 3 followed by a statistical analysis of the errors in Table I. All the analytical polarizabilities within GKS-spRPA were calculated with the def2-QZVPPD basis set with SL PBE potential and 100 frequency grid points. The reference CCSD(T) polarizabilities were calculated numerically using the def2-QZVPPD basis set or are obtained from the numerical CCSD(T) results of Hait and Head-Gordon[82] or the analytical CCSD-F12 calculations of Bokhan *et al.*[83]

The beryllium dimer is a difficult system for standard quantum chemical methods to treat accurately because of the necessity to not only describe long-range dispersion interactions but also static correlation due to the near-degeneracy between the low-lying

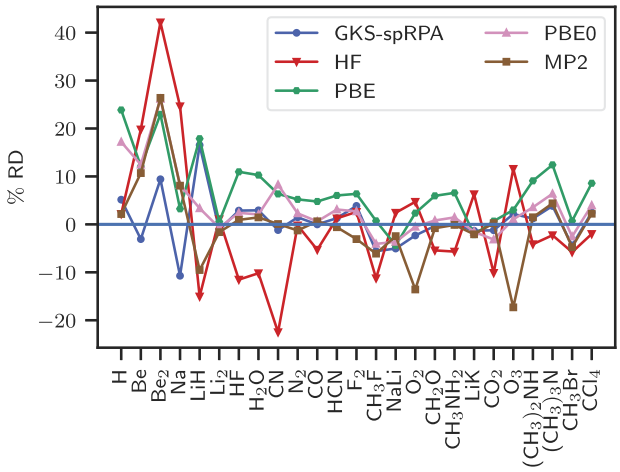


**FIG. 3.** The isotropic static polarizabilities of several small molecules computed using GKS-spRPA are compared with HF, PBE, PBE0, and MP2 methods using the def2-QZVPPD basis set for all of the systems and methods.

excited states.[84] We had previously shown that the ground state potential energy surface of this system is much more accurately described by GKS-spRPA compared to post-KS RPA, optimized effective potential RPA (OEP-RPA),[85] MP2 and SL DFAs.[51] The %RD of the GKS-spRPA polarizabilities from the reference CCSD(T) for $Be_2$, is found to be 9% while for HF it is 42%. PBE, PBE0, and MP2 have %RDs of 22%, 26%, and 27%, respectively. This shows that the accurate description of the energetics of $Be_2$ at the equilibrium bond distance by GKS-spRPA is also replicated for static polarizabilities.

The error analysis in Table I shows that the MAEs are the smallest for GKS-spRPA, followed by MP2, PBE0, PBE, and HF. GKS-spRPA includes first-order exact exchange and correlation of the ring type up to infinite order.[86] These particle–hole excitations are important to describe the polarization of electronic density, and that is part of the reason for GKS-spRPA being successful in predicting the static polarizabilities of these systems.

### D. Conjugated polymers

Local and semilocal DFAs predict incorrect polarizabilities and hyperpolarizabilities of conjugated molecules due to overpolarization problems that worsen with conjugation length.[26,28] This has been attributed to the absence of a field-induced counteracting term in the response part of the XC potential in (semi)local DFAs.[27] A solution to this problem that was conceived in semiconductor

**TABLE I.** The mean signed error (MSE), mean absolute error (MAE), root mean square error (RMSE), standard deviation (Std. Dev.) and the maximum absolute error (Max AE) in atomic units (a.u.) for the testset of 25 polarizabilities are reported for several different methods. All calculations used the def2-QZVPPD basis set for all the atoms, and the GKS-spRPA used the SL PBE potential.

| | GKS-spRPA | HF | PBE | PBE0 | MP2 |
|---|---|---|---|---|---|
| MSE | −0.92 | 3.56 | 1.70 | 1.35 | 0.63 |
| MAE | 2.34 | 5.42 | 3.08 | 2.74 | 2.77 |
| Std. Dev. | 4.66 | 10.89 | 4.77 | 5.29 | 5.39 |
| Max AE | 17.59 | 40.43 | 17.91 | 20.42 | 20.59 |

physics was the addition of polarization dependent terms to the XC potential, which leads to polarization dependent DFT (PDDFT),[36] but the PDDFT XC kernels are unknown and the method has been applied usually for semiconductors where the susceptibility is overestimated by ~10%, whereas for conjugated polymers, the polarizability overestimations can be much larger.[26]

Yang and co-workers[29,87] used the OEP exchange functional (OEP-EXX)[88] for calculating polarizabilities of conjugated oligomers and observed that their results were in good agreement with HF results. They concluded that the OEP-EXX procedure includes "ultranonlocal" exchange effects that are missing in (semi)local DFAs, but OEP-EXX still misses significant contributions from nonlocal long-range correlations. Nénon *et al.*[37] investigated the accuracy of tuned RSHs for calculating the static polarizabilities of polydiacetylene (PDA) and polybutatriene (PBT) oligomers, see Fig. 4, and concluded that the RSH functionals with larger tuning parameters performed better than the ones with smaller tuning parameters. Oviedo *et al.*[89] also performed tuned RSH calculations on PDA and PBT oligomers and found that with very large tuning parameters, broken-symmetry solutions for PBT oligomers are obtained, which results in more accurate polarizabilities than the closed-shell singlet solutions that they obtain with smaller tuning parameters.

For these systems, the SL DFAs result in increasingly smaller HOMO–LUMO gaps as the system size increases, which is depicted in Fig. 5. As the gap gets closer to zero, the static polarizability starts to become divergent for (semi)local DFAs.

The %RDs in longitudinal static polarizabilities of conjugated polymers with respect to reference CCSD(T)-F12 results[89] are reported in Fig. 6. To investigate the effect of orbital optimization, post-PBE polarizabilities obtained from five-point numerical finite differences of energies (with a step size of 0.001 a.u. for the electric field) are also shown. The GKS-spRPA and post-KS RPA results were obtained with a semilocal PBE potential, a def2-TZVPPD basis set, DFT numerical integration grids of size 4[90], and 60 frequency grid points. The PBE and HF calculations were also carried out with

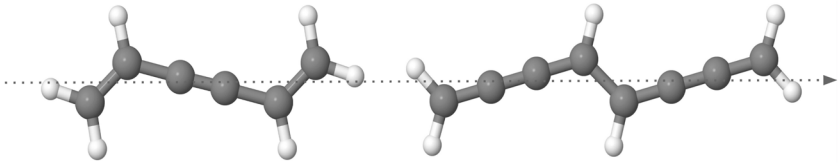

**FIG. 4.** Structures of the polydiacetylene oligomer (PDA1, left) and polybutatriene oligomer (PBT2, right) as well as the longitudinal axis along which the polarizabilities were calculated.

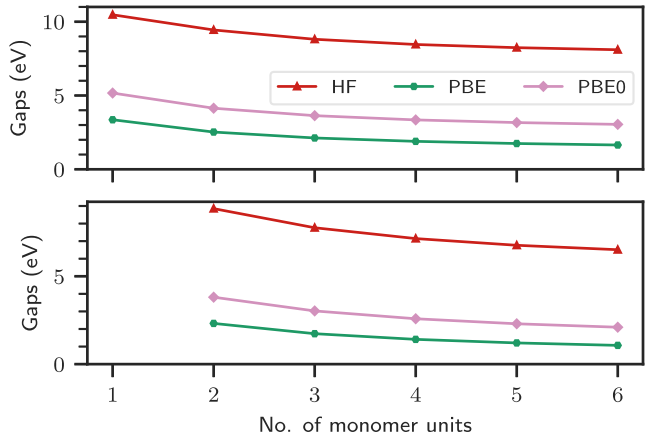


**FIG. 5.** KS semilocal (PBE, PBE0) and HF HOMO–LUMO gaps as a function of the number of monomer units of the PDA (top) and PBT (bottom) oligomers.

the def2-TZVPPD basis set, and numerical integration grids of size 4 were used for the PBE calculations. The CAM-B3LYP results, the reference CCSD(T)-F12 results, as well as the optimized geometries of all the molecules, were obtained from Oviedo *et al.*,[89] who used the cc-PVDZ basis set, froze the core electrons, and performed three-point numerical finite field calculations to obtain the numerical CCSD(T)-F12 static polarizabilities.

The percentage errors in static polarizabilities rapidly increase with the system size for the PBE functional. In case of PDA5, the PBE results reach a %RD of ≥100%. The post-PBE RPA polarizabilities, on the other hand, become increasingly too small, particularly for longer PDA chains. The GKS-spRPA errors, on the other hand, are

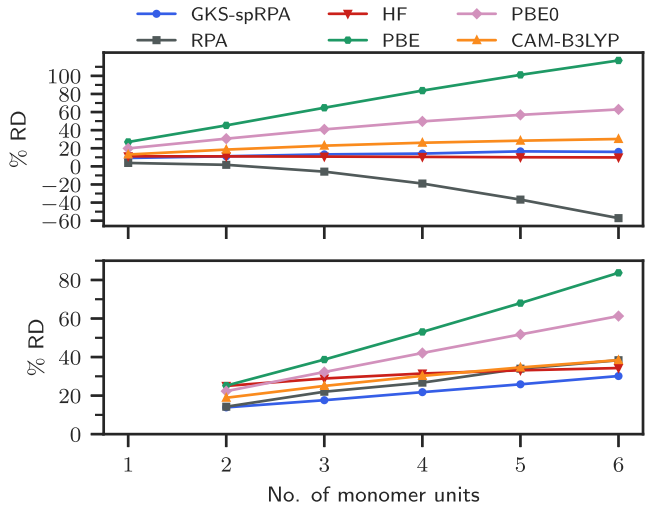


**FIG. 6.** %RD in longitudinal static polarizabilities of PDA (top) and PBT (bottom) oligomers as a function of chain length using CCSD(T)-F12 results from Ref. 89 as reference. def2-TZVPPD basis sets were used throughout; the SL PBE potential and PBE orbitals were used in the GKS-spRPA and post-KS RPA (denoted RPA) calculations.

almost independent of the system size for the PDA oligomers, with a mean %RD of 13%, while RPA, HF, PBE, PBE0, and CAM-B3LYP result in mean %RDs of −19%, 11%, 73%, 43%, and 23%, respectively. For the PBT oligomers, the mean %RD for GKS-spRPA, RPA, HF, PBE, PBE0, and CAM-B3LYP are 22%, 27%, 31%, 54%, 42%, and 29%, respectively. The GKS-spRPA static polarizabilities for both the PDA and PBT oligomers are more accurate than the CAM-B3LYP results, suggesting that the combination of exact HF exchange and long-range correlations contained in the GKS-spRPA functional are responsible for its better performance. HF is accurate for PDA polymers, showing that the net effect of correlation is nearly zero, but the results for other systems studied here suggest that this (somewhat surprising) accuracy of HF may be fortuitous.

Despite the encouraging results for conjugated polymers, the GKS-spRPA is not a functional self-consistent scheme, which means that it has some dependence on the input semilocal DFA through the semicanonical projected semilocal orbital energies [for example in Eq. (12)]. The self-correlation error present in the GKS-spRPA energy functional also contributes to the errors in polarizabilities, which can be partially corrected by including beyond-RPA methods such as the AXK[91] and the SOSEX.[92]

### E. Static polarizabilities of metallocenes

Transition metal metallocenes (TMM) exhibit diverse electronic structures with partially occupied d orbitals and multiple low-lying spin configurations. These properties make them ideal building blocks for molecular spintronic[93] and optoelectronic[94] devices. Theoretical predictions of the polarizabilities of TMMs would help in designing and tuning the properties of these advanced devices. However, TMMs pose challenges to conventional quantum chemical methods because of the small HOMO–LUMO gap due to several low-lying spin configurations. Experimental polarizabilities of the $d^6$ metallocenes, namely ferrocene, ruthenocene, and osmocene, were obtained using gas-phase refractivity measurements by Hohm *et al.*[53,95] Experimental polarizabilities include contributions due to effects such as vibrations and rotations, which can be significant[96,97] and thus must be estimated for accurate comparisons. Ensemble averaged polarizabilities of TMMs were obtained from configurations sampled using *ab initio* molecular dynamics (AIMD) simulations to estimate the magnitude of these corrections. Classical MD simulations can provide suitable estimates here,[98] because vibrational averaging of electronic polarizabilities is typically the main effect.[99] AIMD simulations were run for a total of 10 ps with a time step of 40 a.u. with random initial velocities corresponding to a temperature of 300 K. The TPSS DFA was used along with the def2-SVP basis set for all atoms. After an initial equilibration period of 1 ps, 50 random snapshots were chosen and the average polarizability for this ensemble ($\bar{\alpha}_{iso}$) was calculated within the PBE and PBE0 DFAs using the def2-TZVPPD basis set. Furthermore, geometry optimized structures for TMMs reported by Kehry *et al.*[100] were used to calculate their polarizabilities ($\alpha_{iso}$) using the same DFAs and the difference $\bar{\alpha}_{iso} - \alpha_{iso}$ provides an estimate of the vibrational correction to the polarizabilities. Table II shows that the estimated vibrational corrections ($\bar{\alpha}_{iso} - \alpha_{iso}$) for a given TMM are similar (within 0.4 a.u.) when using the PBE and PBE0 DFAs. Estimates for the purely electronic polarizability of the TMMs, $\alpha^{el}_{exp}$, were obtained by subtracting the thus obtained correction

**TABLE II.** Estimated vibrationally averaged polarizabilities $\bar{\alpha}_{iso}$, $\alpha_{iso}$, and their difference (diff = $\bar{\alpha}_{iso} - \alpha_{iso}$) in a.u. for ferrocene, osmocene, and ruthenocene using the PBE and the PBE0 DFAs.

| | PBE | | | PBE0 | | |
|---|---|---|---|---|---|---|
| | $\bar{\alpha}_{iso}$ | $\alpha_{iso}$ | Diff | $\bar{\alpha}_{iso}$ | $\alpha_{iso}$ | Diff |
| Ferrocene | 131.0 | 127.7 | 3.4 | 123.7 | 120.7 | 3.0 |
| Ruthenocene | 140.2 | 136.0 | 4.2 | 135.0 | 130.9 | 4.1 |
| Osmocene | 141.8 | 136.0 | 5.8 | 136.8 | 131.2 | 5.6 |

**TABLE III.** Isotropic electronic polarizabilities (a.u.) for ferrocene, osmocene, and ruthenocene using various theoretical methods as compared to the estimated experimental value $\alpha_{exp}^{el}$.

| | GKS-spRPA | HF | MP2 | PBE | PBE0 | BSE | $\alpha_{exp}^{el}$ |
|---|---|---|---|---|---|---|---|
| Ferrocene | 123.8 | 107.9 | 124.0 | 127.7 | 120.7 | 131.3 | 123.1 |
| Ruthenocene | 132.2 | 121.3 | 137.4 | 136.0 | 130.9 | 134.2 | 129.0 |
| Osmocene | 132.1 | 122.8 | 136.3 | 136.0 | 131.2 | 137.9 | 132.3 |

using the PBE0 DFA from the experimental polarizabilities by Hohm *et al.*

The GKS-spRPA method was used subsequently to calculate $\boldsymbol{\alpha}$ for the three metallocenes using the geometries reported by Kehry *et al.*[100] who calculated the GW-BSE based static polarizabilities of these molecules. The ground state minimum energy structures of the metallocenes, optimized using the PBE0 functional, were found to have the eclipsed conformation, as shown in Fig. 7. The ground spin states of all these compounds were found to be singlets. GKS-spRPA polarizability calculations were carried out using the PBE SL potential, the def2-TZVPPD basis set for all the atoms along with scalar relativistic effective core potential def2-ECP[101] for the transition metal atoms Ru and Os with a size 4 DFT integration grid[90] and 60 frequency grid points. Additionally, HF, MP2, PBE, and PBE0 calculations were performed with the same basis set and DFT grid as was used for the GKS-spRPA calculations. The thus obtained polarizabilities are reported in Table III. The GKS-spRPA results differ by at most 3.2 a.u. from the experimental values for all three compounds, which is within the error margin of our estimated experimental values. The MP2, PBE, and PBE0 polarizabilities follow a similar pattern as the GKS-spRPA ones but are less accurate, while the HF polarizabilities are considerably too small, and the GW-BSE@DFA results are too large.

### F. Static polarizabilities of sodium clusters

Experimental static polarizabilities of alkali metal clusters, such as sodium and lithium clusters are known to have large uncertainties and poor reproducibility.[102,103] For example, from $Na_6$ to $Na_7$, the isotropic static polarizability ($\alpha_{iso}$) according to Rayane *et al.*,[102] decreases from 816.62 to 800.69, whereas there is an increase observed by Knight *et al.*,[103] from 754.42 to 808.34. Both Knight *et al.*, and Rayane *et al.* used molecular beam deflection of the $Na_n$ clusters through a static inhomogeneous transverse electric field to measure the $\alpha_{iso}$ of the $Na_n$ clusters. Accurate theoretical calculations of the polarizabilities of these systems could resolve the uncertain experimental results.

Previous theoretical studies based on MP2 by Chandrakumar *et al.*,[52] also suggest a decrease in the $\alpha_{iso}$ going from $Na_6$ to $Na_7$, while HF suggests an increase. These clusters are difficult systems because they can have multiple nearly degenerate local minimum energy structures in the ground state. Furthermore, clusters with odd numbers of electrons can have multiple nearly degenerate spin states that further complicate the electronic structure. Therefore, accurate theoretical benchmark calculations taking into account the fluxional nature of the metal cluster structures are necessary, especially since these experiments are typically done at finite temperatures.

In this study, the GKS-spRPA $\alpha_{iso}$ are benchmarked for small $Na_n$ clusters ($n = 2, 3, \ldots, 10$) and we aim to answer two questions: (i) Can GKS-spRPA predict the experimentally observed trends accurately, and (ii) how important are thermal contributions to $\alpha_{iso}$? To answer the first question, the geometries of the $Na_n$ clusters were optimized to acquire local minimum energy structures, see Fig. 8, and then $\alpha_{iso}$ was calculated for these structures to obtain the zero temperature results. Geometry optimization calculations were carried out within the DFT using the B3-LYP functional and the def2-TZVPP basis set for the Na atoms, and grid size 4 was used along

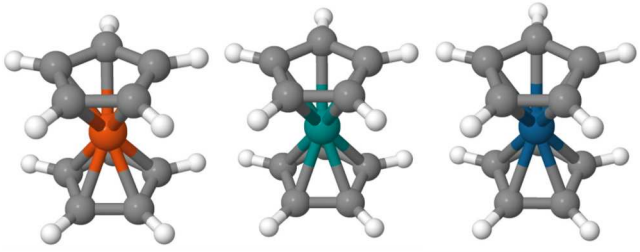

**FIG. 7.** Structures of ferrocene [$Fe(C_5H_5)_2$], ruthenocene [$Ru(C_5H_5)_2$] and osmocene [$Os(C_5H_5)_2$] (left to right).

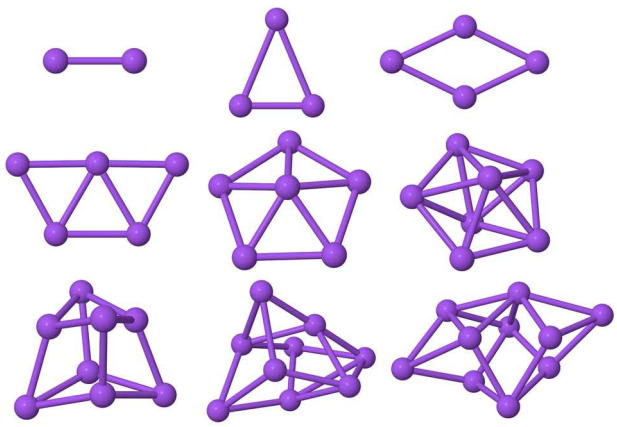

**FIG. 8.** Structures of sodium clusters optimized with the B3-LYP[104] DFA using the def2-TZVPP basis set. Normal mode analysis is performed to confirm that these are local minimum energy structures.

with weight derivatives. To address the second question, *ab initio* molecular dynamics (AIMD) calculations were performed to simulate the equilibrium dynamics of the $Na_n$ clusters, and using these AIMD trajectories, 50 snapshots were randomly selected from which the trajectory averaged polarizabilities ($\bar{\alpha}_{iso}$) were calculated. The AIMD simulations were carried out using the B3-LYP functional and the def2-TZVPP basis sets. A microcanonical ensemble was used for the simulation of ground state equilibrium dynamics, ensuring conservation of energy. The AIMD simulations were run for a total of 10 ps with a 20 a.u. timestep. The first 1ps of the trajectory was not used for sampling to allow the system to attain equilibrium, and from the remaining 9 ps, 50 snapshots were selected at random and used for the calculation of $\bar{\alpha}_{iso}$. The minimum/maximum deviations as well as the average absolute deviations (AAD) of $\alpha_{iso}$ and $\bar{\alpha}_{iso}$ from experimental polarizabilities are reported in Table IV. For the local minimum energy structures, HF and PBE polarizabilities can vary from being overestimated to underestimated with an AAD of 74 and 86 a.u., respectively. GKS-spRPA polarizabilities are systematically underestimated with an AAD of 95 a.u.. The ensemble averaged polarizabilities calculated using HF have maximum and minimum deviations of 450.0 and −203.9 a.u., respectively, which is quite large. The difference between the AAD of $\alpha_{iso}$ and $\bar{\alpha}_{iso}$ can be associated with the average thermal correction to the calculated polarizabilities. $\bar{\alpha}_{iso}$ on average worsens the $\alpha_{iso}$ by 10 a.u. with the inclusion of structural fluctuations using the HF method. However, using GKS-spRPA and PBE, the polarizabilities are improved by 15 and 8 a.u. on average. These results suggest that thermal effects are not significant in determining the polarizabilities of the $Na_n$ clusters. The distribution of the polarizabilities calculated from the AIMD snapshots are represented in Fig. 9 as box plots. It can be observed that the spread in the $\bar{\alpha}_{iso}$ calculated using HF is considerably larger for clusters with odd number of atoms, which have an open-shell ground state electronic configuration than it is for clusters with even number of atoms. Some of the $Na_3$ AIMD snapshots resulted in $\alpha_{iso}$of ~ 900 a.u. using HF, which is qualitatively incorrect compared to the experimental results, which are ≤500 a. u. for the $Na_3$ cluster. The spread in the GKS-spRPA results is independent of whether the cluster has an odd or even number of Na atoms, and none of the AIMD snapshots resulted in qualitative overestimation of $\alpha_{iso}$,

**TABLE IV.** Calculated minimum/maximum deviations (Min/Max) and the average absolute deviation (AAD) of the isotropic polarizabilities (a.u.) for the geometry optimized (Opt.) and AIMD structures of the $Na_n$ ($n = \{3, \ldots, 10\}$) clusters using the GKS-spRPA, HF and PBE methods compared to the experimental results. The deviations are calculated as $\bar{\alpha}_{iso}^{calc} - \alpha_{iso}^{expt}$, where *calc* and *expt* refers to calculated and experimental polarizabilities (average of the polarizabilities reported by Knight *et al.*[103] and Rayane *et al.*[102]), respectively.

| | | GKS-spRPA | HF | PBE |
|---|---|---|---|---|
| Opt. | Min | −262.5 | −191.7 | −285.6 |
| | Max | −28.0 | 156.9 | 46.8 |
| | AAD | 94.8 | 74.4 | 85.7 |
| AIMD | Min | −278.6 | −203.9 | −285.6 |
| | Max | 36.9 | 450.0 | 46.8 |
| | AAD | 79.9 | 74.4 | 85.7 |

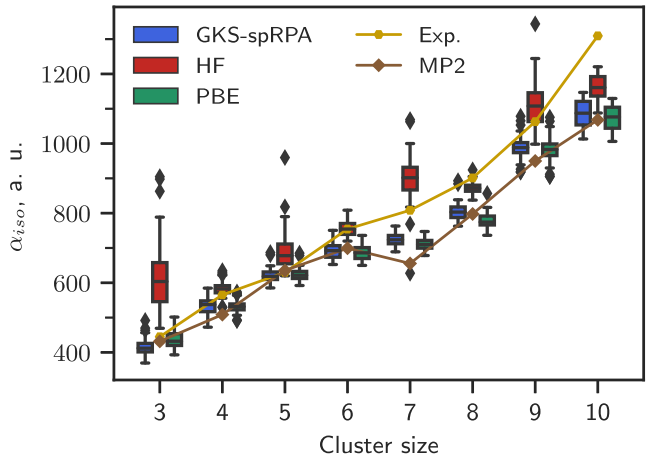


**FIG. 9.** Calculated $\alpha_{iso}$ using GKS-spRPA, PBE, and HF methods in a.u. for the 50 snapshots from the AIMD simulations are represented as box plots. The box represents the interquartile range (IQR), which is from the 25th (first quartile, Q1) to the 75th (third quartile, Q3) percentile of the data, and the line inside the box represents the median. The whiskers denote Q1 −1.5× IQR and Q3 +1.5× IQR and data points that lie outside this range are denoted by solid black diamonds.

as is the case with HF. In addition to temperature effects, the discrepancy between the calculated and measured polarizabilities for the $Na_n$ clusters has been attributed to errors in experiments, which can arise because the accuracy of the measurements depends upon several parameters used in the experimental setup.[52]

We compared the polarizabilities obtained within the GKS-spRPA method for the $Na_n$ clusters to the numerical finite field MP2 calculations reported by Chandrakumar and co-workers.[52] According to Fig. 9, the MP2 $\alpha_{iso}$ values show a spurious decrease from $Na_6$ (699 a.u.) to $Na_7$ (655 a.u.), whereas they increase for the GKS-spRPA method (675 and 715 a.u., respectively) and the experiment. The average absolute deviation of $\alpha_{iso}$ within GKS-spRPA is 27 a.u. compared to the MP2 results. In conclusion, GKS-spRPA polarizabilities are more accurate than those of HF and are comparable to PBE, and both of these methods (PBE and GKS-spRPA) result in systematic underestimations of the polarizabilities for $Na_n$ clusters.

## V. CONCLUSIONS

An analytical implementation of static GKS-spRPA polarizabilities within the RI approximation with $\mathcal{O}(N^4 \log N)$ floating point operation count and $\mathcal{O}(N^3)$storage has been presented. The basis-set requirements are similar to those encountered with HF, DFAs, and MP2: Property optimized def2-TZVPPD and QZVPPD basis sets[7,105] yield converged GKS-spRPA polarizabilities with %RDs of ≤1% relative to the basis set limit. For small molecules, the GKS-spRPA polarizabilities are more accurate than the HF, MP2, PBE, PBE0, and nonselfconsistent RPA ones when compared to CCSD(T). A key finding is that GKS-spRPA addresses the problem of overpolarization encountered by SL/hybrid DFAs for $\pi$-conjugated systems, certainly at a qualitative level. Post-PBE RPA, on the other hand, severely underestimates the static polarizabilities of longer conjugated polymers, suggesting that orbital optimization

is critical for accurate response properties. For the systems considered here, GKS-spRPA polarizabilities are also more accurate than RSH polarizabilities, at least without molecule-specific "tuning."[37,40] This may be attributed to the inclusion of (100% of) exact HF exchange and long-range correlation effects, which are only partially or not at all present in RSHs. For ferrocene and its heavier cogeners, GSK-spRPA polarizabilities clearly outperform previously reported GW-BSE ones after vibrational corrections are included. The isotropic static polarizabilities of small sodium clusters ($\alpha_{iso}$), calculated using local minimum energy structures, and the ensemble averaged isotropic static polarizabilities ($\bar{\alpha}_{iso}$), calculated using AIMD ensemble averaging, were found to qualitatively agree with experiments and showed a monotonic increase with cluster size. Thermal averaging improved the results by 15 a.u. using the GKS-spRPA method, indicating that thermal effects play a minor role for static polarizabilities of these clusters. The more systematic behavior of GKS-spRPA polarizabilities compared to MP2 mirrors findings for dispersion energies[106] and is more pronounced for large and highly polarizable systems.

GKS-spRPA still violates the "flat plane condition"[107] due to residual self-correlation error, although orbital self-consistency is likely to reduce its effects on properties. Apart from the sp approximation, this may be a major source of error in the present approach. The magnitude of the latter could be explored using beyond-RPA methods, including second-order exchange, such as AXK[91] and SOSEX.[92] In summary, the results presented here suggest that GKS-spRPA is a step toward electronic structure methods yielding consistently accurate response properties for diverse molecular systems at an affordable cost.

## SUPPLEMENTARY MATERIAL

See the supplementary material for a detailed derivation of analytical second derivatives of the RPA energy Lagrangian, explicit expressions for intermediate quantities, detailed numerical results, and optimized geometries.

## ACKNOWLEDGMENTS

This work was supported by the National Science Foundation under Grant Nos. CHE-1800431 and CHE-2102568.

## AUTHOR DECLARATIONS

### Conflict of Interest

Principal Investigator Filipp Furche has an equity interest in TURBOMOLE GmbH. The terms of this arrangement have been reviewed and approved by the University of California, Irvine, in accordance with its conflict of interest policies.

### Author Contributions

**Sree Ganesh Balasubramani**: Conceptualization (equal); Data curation (lead); Formal analysis (equal); Investigation (lead); Methodology (equal); Software (lead); Validation (lead); Visualization (lead); Writing – original draft (lead). **Vamsee K. Voora**: Conceptualization (equal); Data curation (equal); Formal analysis (equal); Investigation (equal); Methodology (equal); Software (equal); Supervision (supporting); Validation (lead); Visualization (supporting); Writing – review & editing (equal). **Filipp Furche**: Conceptualization (lead); Data curation (supporting); Formal analysis (equal); Funding acquisition (lead); Methodology (equal); Project administration (lead); Resources (lead); Software (equal); Supervision (lead); Validation (equal); Writing – original draft (supporting); Writing – review & editing (equal).

## DATA AVAILABILITY

The data that support the findings of this study are available within the article and its supplementary material.

## REFERENCES

[1] S. Mukamel, *Principles of Nonlinear Optical Spectroscopy*, Oxford series in optical and imaging sciences (Oxford University Press, 1995).
[2] M. G. Papadopoulos, A. Sadlej, and J. Leszczynski, *Non-Linear Optical Properties of Matter*, Challenges and Advances in Computational Chemistry and Physics (Springer, Dordrecht, 2006).
[3] J. F. Stanton and R. J. Bartlett, J. Chem. Phys. **99**, 5178 (1993).
[4] A. J. Sadlej, Chem. Phys. Lett. **47**, 50 (1977).
[5] A. J. Sadlej and M. Urban, J. Mol. Struct.: THEOCHEM **234**, 147 (1991).
[6] F. Jensen, J. Chem. Theory Comput. **4**, 719 (2008).
[7] D. Rappoport and F. Furche, J. Chem. Phys. **133**, 134105 (2010).
[8] D. M. Bishop, Rev. Mod. Phys. **62**, 343 (1990).
[9] H. Sekino and R. J. Bartlett, J. Chem. Phys. **85**, 976 (1986).
[10] M. Feyereisen, J. Nichols, J. Oddershede, and J. Simons, J. Chem. Phys. **96**, 2978 (1992).
[11] H. Weiss, R. Ahlrichs, and M. Häser, J. Chem. Phys. **99**, 1262 (1993).
[12] E. D. Simandiras, R. D. Amos, and N. C. Handy, Chem. Phys. **114**, 9 (1987).
[13] J. E. Rice and N. C. Handy, J. Chem. Phys. **94**, 4959 (1991).
[14] H. Koch and P. Jørgensen, J. Chem. Phys. **93**, 3333 (1990).
[15] C. Haettig and A. Köhn, J. Chem. Phys. **117**, 6939 (2002).
[16] D. H. Friese, N. O. C. Winter, P. Balzerowski, R. Schwan, and C. Hättig, J. Chem. Phys. **136**, 174106 (2012).
[17] J. R. Hammond, K. Kowalski, and W. A. deJong, J. Chem. Phys. **127**, 144105 (2007).
[18] T. Helgaker, S. Coriani, P. Jørgensen, K. Kristensen, J. Olsen, and K. Ruud, Chem. Rev. **112**, 543 (2012).
[19] P. Hohenberg and W. Kohn, Phys. Rev. **136**, B864 (1964).
[20] K. Burke, J. Chem. Phys. **136**, 150901 (2012).
[21] W. Kohn and L. J. Sham, Phys. Rev. **140**, A1133 (1965).
[22] A. Seidl, A. Görling, P. Vogl, J. A. Majewski, and M. Levy, Phys. Rev. B **53**, 3764 (1996).
[23] S. J. A. van Gisbergen, J. G. Snijders, and E. J. Baerends, Phys. Rev. Lett. **78**, 3097 (1997).
[24] R. Bauernschmitt and R. Ahlrichs, Chem. Phys. Lett. **256**, 454 (1996).
[25] D. Rappoport and F. Furche, J. Chem. Phys. **122**, 064105 (2005).
[26] B. Champagne, E. A. Perpète, S. J. A. van Gisbergen, E.-J. Baerends, J. G. Snijders, C. Soubra-Ghaoui, K. A. Robins, and B. Kirtman, J. Chem. Phys. **109**, 10489 (1998).
[27] S. J. A. van Gisbergen, P. R. T. Schipper, O. V. Gritsenko, E. J. Baerends, J. G. Snijders, B. Champagne, and B. Kirtman, Phys. Rev. Lett. **83**, 694 (1999).
[28] B. Champagne, E. A. Perpète, D. Jacquemin, S. J. A. van Gisbergen, E.-J. Baerends, C. Soubra-Ghaoui, K. A. Robins, and B. Kirtman, J. Phys. Chem. A **104**, 4755 (2000).
[29] P. Mori-Sánchez, Q. Wu, and W. Yang, J. Chem. Phys. **119**, 11001 (2003).
[30] M. van Faassen, P. L. de Boeij, R. van Leeuwen, J. A. Berger, and J. G. Snijders, Phys. Rev. Lett. **88**, 186401 (2002).
[31] J. P. Perdew and A. Zunger, Phys. Rev. B **23**, 5048 (1981).
[32] C. D. Pemmaraju, S. Sanvito, and K. Burke, Phys. Rev. B **77**, 121204 (2008).

[33]A. J. Cohen, P. Mori-Sánchez, and W. Yang, Chem. Rev. **112**, 289 (2012).
[34]B. Kirtman, S. Bonness, A. Ramirez-Solis, B. Champagne, H. Matsumoto, and H. Sekino, J. Chem. Phys. **128**, 114108 (2008).
[35]P. A. Limacher, K. V. Mikkelsen, and H. P. Lüthi, J. Chem. Phys. **130**, 194114 (2009).
[36]W. G. Aulbur, L. Jönsson, and J. W. Wilkins, Phys. Rev. B **54**, 8540 (1996).
[37]S. Nénon, B. Champagne, and M. I. Spassova, Phys. Chem. Chem. Phys. **16**, 7083 (2014).
[38]C. Adamo and V. Barone, J. Chem. Phys. **110**, 6158 (1999).
[39]A. J. Garza, N. A. Wazzan, A. M. Asiri, and G. E. Scuseria, J. Phys. Chem. A **118**, 11787 (2014).
[40]L. Kronik, T. Stein, S. Refaely-Abramson, and R. Baer, J. Chem. Theory Comput. **8**, 1515 (2012).
[41]A. J. Garza, O. I. Osman, A. M. Asiri, and G. E. Scuseria, J. Phys. Chem. B **119**, 1202 (2015).
[42]D. C. Langreth and J. P. Perdew, Phys. Rev. B **15**, 2884 (1977).
[43]F. Furche, Phys. Rev. B **64**, 195120 (2001).
[44]G. P. Chen, V. K. Voora, M. M. Agee, S. G. Balasubramani, and F. Furche, Annu. Rev. Phys. Chem. **68**, 421 (2017).
[45]A. M. Burow, J. E. Bates, F. Furche, and H. Eshuis, J. Chem. Theory Comput. **10**, 180 (2014).
[46]B. Ramberger, T. Schäfer, and G. Kresse, Phys. Rev. Lett. **118**, 106403 (2017).
[47]M. Beuerle and C. Ochsenfeld, J. Chem. Phys. **149**, 244111 (2018).
[48]A. Thierbach and A. Görling, J. Chem. Phys. **153**, 134113 (2020).
[49]J. M. Yu, B. D. Nguyen, J. Tsai, D. J. Hernandez, and F. Furche, J. Chem. Phys. **155**, 040902 (2021).
[50]H. Eshuis, J. Yarkony, and F. Furche, J. Chem. Phys. **132**, 234114 (2010).
[51]V. K. Voora, S. G. Balasubramani, and F. Furche, Phys. Rev. A **99**, 012518 (2019).
[52]K. R. S. Chandrakumar, T. K. Ghanty, and S. K. Ghosh, J. Chem. Phys. **120**, 6487 (2004).
[53]U. Hohm, D. Goebel, and S. Grimme, Chem. Phys. Lett. **272**, 328 (1997).
[54]F. Weigend, M. Häser, H. Patzelt, and R. Ahlrichs, Chem. Phys. Lett. **294**, 143 (1998).
[55]N. C. Handy, R. D. Amos, J. F. Gaw, J. E. Rice, and E. D. Simandiras, Chem. Phys. Lett. **120**, 151 (1985).
[56]M. Head-Gordon and T. Head-Gordon, Chem. Phys. Lett. **220**, 122 (1994).
[57]M. Kollwitz and J. Gauss, Chem. Phys. Lett. **260**, 639 (1996).
[58]J. P. Perdew, W. Yang, K. Burke, Z. Yang, E. K. U. Gross, M. Scheffler, G. E. Scuseria, T. M. Henderson, I. Y. Zhang, A. Ruzsinszky, H. Peng, J. Sun, E. Trushin, and A. Görling, Proc. Natl. Acad. Sci. U. S. A. **114**, 2801 (2017).
[59]H. Eshuis, J. E. Bates, and F. Furche, Theor. Chem. Acc. **131**, 1084 (2012).
[60]M.-C. Kim, E. Sim, and K. Burke, Phys. Rev. Lett. **111**, 073003 (2013).
[61]A. Wasserman, J. Nafziger, K. Jiang, M.-C. Kim, E. Sim, and K. Burke, Annu. Rev. Phys. Chem. **68**, 555 (2017).
[62]A. Szabo and N. Ostlund, *Modern Quantum Chemistry: Introduction to Advanced Electronic Structure Theory*, Dover Books on Chemistry (Dover Publications, 1996).
[63]F. Furche and R. Ahlrichs, J. Chem. Phys. **117**, 7433 (2002).
[64]V. K. Voora, R. Galhenage, J. C. Hemminger, and F. Furche, J. Chem. Phys. **151**, 134106 (2019).
[65]V. K. Voora, J. Phys. Chem. Lett. **12**, 433 (2021).
[66]P. Pulay, "Analytical derivative methods in quantum chemistry," in *Advances in Chemical Physics* (John Wiley & Sons, 2007), pp. 241–286.
[67]E. P. Wigner, "On a modification of the Rayleigh-Schrödinger perturbation theory," in *Part I: Physical Chemistry. Part II: Solid State Physics*, edited by A. S. Wightman (Springer Berlin Heidelberg, Berlin, Heidelberg, 1997) pp. 131–136
[68]S. T. Esptein, *The Variation Method in Quantum Chemistry* (Elsevier, 1974), Vol. 33.
[69]J. Gerratt and I. M. Mills, J. Chem. Phys. **49**, 1730 (1968).
[70]T. U. Helgaker and J. Almlöf, Int. J. Quantum Chem. **26**, 275 (1984).
[71]J. A. Pople, R. Krishnan, H. B. Schlegel, and J. S. Binkley, Int. J. Quantum Chem. **16**, 225 (1979).
[72]P. Deglmann, F. Furche, and R. Ahlrichs, Chem. Phys. Lett. **362**, 511 (2002).
[73]F. Furche, J. Chem. Phys. **114**, 5982 (2001).
[74]F. London, J. Phys. Radium **8**, 397 (1937).
[75]R. Ditchfield, Mol. Phys. **27**, 789 (1974).
[76]E. R. Davidson, J. Comput. Phys. **17**, 87 (1975).
[77]T. D. Bouman, A. E. Hansen, B. Voigt, and S. Rettrup, Int. J. Quantum Chem. **23**, 595 (1983).
[78]J. Olsen, H. J. A. Jensen, and P. Jørgensen, J. Comput. Phys. **74**, 265 (1988).
[79]F. Furche, B. T. Krull, B. D. Nguyen, and J. Kwon, J. Chem. Phys. **144**, 174105 (2016).
[80]S. G. Balasubramani, G. P. Chen, S. Coriani, M. Diedenhofen, M. S. Frank, Y. J. Franzke, F. Furche, R. Grotjahn, M. E. Harding, C. Hättig, A. Hellweg, B. Helmich-Paris, C. Holzer, U. Huniar, M. Kaupp, A. Marefat Khah, S. Karbalaei Khani, T. Müller, F. Mack, B. D. Nguyen, S. M. Parker, E. Perlt, D. Rappoport, K. Reiter, S. Roy, M. Rückert, G. Schmitz, M. Sierka, E. Tapavicza, D. P. Tew, C. van Wüllen, V. K. Voora, F. Weigend, A. Wodyński, and J. M. Yu, J. Chem. Phys. **152**, 184107 (2020).
[81]*NIST Computational Chemistry Comparison and Benchmark Database*, NIST Standard Reference Database Number 101, Release 22, May 2022, Editor: Russell D. Johnson III, http://cccbdb.nist.gov/.
[82]D. Hait and M. Head-Gordon, Phys. Chem. Chem. Phys. **20**, 19800 (2018).
[83]D. Bokhan, D. N. Trubnikov, A. Perera, and R. J. Bartlett, J. Chem. Phys. **145**, 134104 (2016).
[84]S. Sharma, T. Yanai, G. H. Booth, C. J. Umrigar, and G. K.-L. Chan, J. Chem. Phys. **140**, 104112 (2014).
[85]N. L. Nguyen, N. Colonna, and S. de Gironcoli, Phys. Rev. B **90**, 045138 (2014).
[86]M. Gell-Mann and K. A. Brueckner, Phys. Rev. **106**, 364 (1957).
[87]F. A. Bulat, A. Toro-Labbé, B. Champagne, B. Kirtman, and W. Yang, J. Chem. Phys. **123**, 014319 (2005).
[88]W. Yang and Q. Wu, Phys. Rev. Lett. **89**, 143002 (2002).
[89]M. B. Oviedo, N. V. Ilawe, and B. M. Wong, J. Chem. Theory Comput. **12**, 3593 (2016).
[90]O. Treutler and R. Ahlrichs, J. Chem. Phys. **102**, 346 (1995).
[91]J. E. Bates and F. Furche, J. Chem. Phys. **139**, 171103 (2013).
[92]A. Grüneis, M. Marsman, J. Harl, L. Schimka, and G. Kresse, J. Chem. Phys. **131**, 154115 (2009).
[93]R. Liu, S.-H. Ke, H. U. Baranger, and W. Yang, Nano Lett. **5**, 1959 (2005).
[94]A. Ishii and T. Miyasaka, Chem. Phys. Chem. **15**, 1028 (2014).
[95]D. Goebel and U. Hohm, J. Chem. Soc., Faraday Trans. **93**, 3467 (1997).
[96]M. J. Cohen, A. Willetts, R. D. Amos, and N. C. Handy, J. Chem. Phys. **100**, 4467 (1994).
[97]D. M. Bishop, J. Pipin, and B. Kirtman, J. Chem. Phys. **102**, 6778 (1995).
[98]A. Osted, J. Kongsted, K. V. Mikkelsen, P.-O. Åstrand, and O. Christiansen, J. Chem. Phys. **124**, 124503 (2006).
[99]D. M. Bishop and B. Kirtman, J. Chem. Phys. **95**, 2646 (1991).
[100]M. Kehry, Y. J. Franzke, C. Holzer, and W. Klopper, Mol. Phys. **118**, e1755064 (2020).
[101]D. Andrae, U. Häußermann, M. Dolg, H. Stoll, and H. Preuß, Theor. Chem. Acc. **77**, 123 (1990).
[102]D. Rayane, A. R. Allouche, E. Benichou, R. Antoine, M. Aubert-Frecon, P. Dugourd, M. Broyer, C. Ristori, F. Chandezon, B. A. Huber, and C. Guet, Eur. Phys. J. D **9**, 243 (1999).
[103]W. D. Knight, K. Clemenger, W. A. de Heer, and W. A. Saunders, Phys. Rev. B **31**, 2539 (1985).
[104]A. D. Becke, J. Chem. Phys. **98**, 5648 (1993).
[105]D. Rappoport, J. Chem. Phys. **155**, 124102 (2021).
[106]B. D. Nguyen, G. P. Chen, M. M. Agee, A. M. Burow, M. P. Tang, and F. Furche, J. Chem. Theory Comput. **16**, 2258 (2020).
[107]P. Mori-Sánchez, A. J. Cohen, and W. Yang, Phys. Rev. Lett. **102**, 066403 (2009).